Dynamically strained ferroelastics: Statistical behavior in elastic and plastic regimes

X. Ding,[1,2,*] T. Lookman,[2] Z. Zhao,[1] A. Saxena,[2] J. Sun,[1] and E. K. H. Salje[2,3,*]

[1]*State Key Laboratory for Mechanical Behavior of Materials, Xi'an Jiaotong University, Xi'an 710049, China*

[2]*Theoretical Division and Center for Nonlinear Studies, Los Alamos National Laboratory, Los Alamos, New Mexico 87545, USA*

[3]*Department of Earth Sciences, University of Cambridge, Cambridge CB2 3EQ, United Kingdom*

(Received 22 October 2012; published 20 March 2013)

The dynamic evolution in ferroelastic crystals under external shear is explored by computer simulation of a two-dimensional model. The characteristic geometrical patterns obtained during shear deformation include dynamic tweed in the elastic regime as well as interpenetrating needle domains in the plastic regime. As a result, the statistics of jerk energy differ in the elastic and plastic regimes. In the elastic regime the distributions of jerk energy are sensitive to temperature and initial configurations. However, in the plastic regime the jerk distributions are rather robust and do not depend much on the details of the configurations, although the geometrical pattern formed after yield is strongly influenced by the elastic constants of the materials and the configurations we used. Specifically, for all geometrical configurations we studied, the energy distribution of jerks shows a power-law noise pattern $P(E) \sim E^{-(\gamma-1)}(\gamma - 1 = 1.3 - 2)$ at low temperatures and a Vogel-Fulcher distribution $P(E) \sim \exp\text{-}(E/E_0)$ at high temperatures. More complex behavior occurs at the crossover between these two regimes where our simulated jerk distributions are very well described by a generalized Poisson distributions $P(E) \sim E^{-(\gamma-1)}$ $\exp\text{-}(E/E_0)^n$ with $n = 0.4$–0.5 and $\gamma - 1 \approx 0$ (Kohlrausch law). The geometrical mechanisms for the evolution of the ferroelastic microstructure under strain deformation remain similar in all thermal regimes, whereas their thermodynamic behavior differs dramatically: on heating, from power-law statistics via the Kohlrausch law to a Vogel-Fulcher law. There is hence no simple way to predict the local evolution of the twin microstructure from just the observed statistical behavior of a ferroelastic crystal. It is shown that the Poisson distribution is a convenient way to describe the crossover behavior contained in all the experimental data without recourse to specific scaling functions or temperature-dependent cutoff lengths.

DOI: 10.1103/PhysRevB.87.094109 PACS number(s): 64.60.av, 81.30.Kf, 64.70.Nd, 05.50.+q

I. INTRODUCTION

The study of criticality in externally driven inhomogeneous systems without order parameter conservation (model A in the Hohenberg-Halperin taxonomy[1]) has advanced in two directions. First, theoretical considerations have led to the idea of flickering noise and distribution functions for the expectation values of avalanche sizes, their energies, and the power spectra of the excitations.[2,3] Second, such distribution functions have been measured by acoustic emission experiments and direct optical observations of avalanches.[4–7] In this paper we use the term "jerk" to describe any discontinuity in energy leading to so-called avalanches, pinning and depinning events of needle domains, independent of their geometrical origin. Jerks in our computer simulations appear as sudden changes of the energy content of the sample exactly as measured previously in ferroelastic and martensitic materials.[5,6,8] Computer simulations have helped to identify the dynamics of domain movements in ferroelastic and martensitic materials, and we have previously identified the two main regimes.[8,9] At low temperatures, we found power-law distributions of the energy of avalanches. At high temperatures, when the sample is still ferroelastic but approaches the melting point, we found thermally excited Vogel-Fulcher distributions. This result showed that the well-known power-law statistics associated with athermal martensitic behavior is not universal but restricted to low-temperature dynamics, i.e., to temperatures below the Vogel-Fulcher temperature (T_{VF}).[8] The crossover between these two regimes is unknown, and it is the purpose of this study to investigate the distribution function of jerks and analyze how this distribution depends on intrinsic sample properties.

In this paper, we use a two-dimensional model previously studied[8] to explore the driven dynamic behavior of thin ferroelastic films with different elastic constants ($K1$) and different initial configurations. Our model is constructed to be generic for all ferroelastic phase transitions by choosing as order parameter the shear angle, which leads to ferroelastic twinning. This twinning and the mobility of the twin walls defines ferroelasticity.[10] Comparing this configuration with the ferroelastic transition between cubic and tetragonal phases in $SrTiO_3$ at 105 K, we focus on the modeling of a plane perpendicular to the twin plane (i.e., our axes are [101] and $[\bar{1}01]$ of the $Pm\bar{3}m$ setting). Equivalent planes can be found in all ferroelastic systems.[10]

We find that the application of shear in thin ferroelastic films generates complex microstructures, including dynamic tweed in the elastic regime as well as interpenetrating needle domains in the plastic regime. As a result, the statistics of jerk energy in the elastic regime differ from that in the plastic regime, e.g., power-law distributions of jerk energy are observed in the elastic regime, whereas noise in the plastic regime follows stretched exponential distributions. Interestingly, we find that the statistics of jerk energy with its stages of power laws, stretched exponentials, and simple Vogel-Fulcher behavior are rather robust in the plastic regime and do not depend much on the details of the configurations, i.e., for the dynamical distribution function of jerks in the plastic regime, we find that the crossover regime between power law and Vogel-Fulcher region can be best described by a stretched exponential (Kohlrausch) distribution[4] with surprisingly universal stretching exponents.

We suggest experiments to validate our predictions. Previous experimental studies have shown that ferroelastic crystals and martensites do indeed display avalanche properties, which can be seen as jerks or acoustic emission when the samples are subjected to external strain.[5] These experiments are conducted on time scales that are compatible with the time scale of the waiting time between jerks. Our finding is that the observed waiting time statistics in the plastic regime, which may be seen in experiments, follow a generalized Poisson distribution[6,7] $P(t) \sim t^{-(\gamma-1)}$ exp-$(t/\tau)^n$ so that some systems will obey a simple exponential distribution with $\gamma - 1 \approx 0$ and $n = 1$, and others will follow the stretched exponential with $\gamma - 1 \approx 0$ and $n = 0.4$.

This paper is organized as follows: in Sec. II, we briefly introduce the model and methods for our MD simulations. Section III focuses on the results of the MD simulations. We first check the evolution of microstructure under applied shear, and then calculate the statistics of jerk energy in the plastic and elastic regimes. In Sec. IV we compare our results to theoretical predictions and experimental results.

II. THE SIMULATION

Our model is based on interatomic interactions[11] rather than coarse-grained simulations[12] because the elementary step leading to advancing twin boundaries is known to be related to the sideways movement of kinks inside these boundaries.[13] Such atomic scale kinks are well reproduced by atomic scale simulations, whereas coarse-grained methods average over such fine structural details.[14] The interatomic potentials were chosen to reproduce most closely the mesoscopic Landau potentials of the relevant materials.[15–17] As the shear angle of ferroelastic materials[18] is typically below 4° compared with many martensitic materials that often have larger shear angles, we constructed the model so that the shear angle was fixed to 4°, a good compromise for metallic as well as oxide materials. The simulations were conducted with three interactions in a monoatomic, two-dimensional lattice.[8] The three interactions are (1) harmonic nearest-neighbor interactions (elastic springs), $U(r) = K1(r-1)^2$, black springs in Fig. 1; (2) double-well potentials between next-nearest neighbors, $U(r) = -10(r-\sqrt{2})^2 + 2000(r-\sqrt{2})^4$; diagonals in the square lattice, red springs online in Fig. 1; (3) fourth-order interactions (springs) between the third nearest neighbors that are parallel to the nearest-neighbor interactions with $U(r) = -(r-2)^4$ and long dashed green lines in Fig. 1. The elastic constant $K1$ is for the nearest-neighbor interactions, and r is the distance vector. The resulting potential is a sum of the three interactions. The springs (1) and (3) define the elastic background and define the thickness of interfaces. The Landau springs (2) define the double-well potential of the ferroelastic phase transition. They define a second-order phase transition inspired by the transition of $SrTiO_3$.[19] Extensions to other materials are straightforward and would rescale the temperature and the twin angle, while all other parameters remain generic. An extension to first-order phase transitions is easy to implement but does not add anything new because all studies are performed deep in the ferroelastic phase far below the transition temperature.

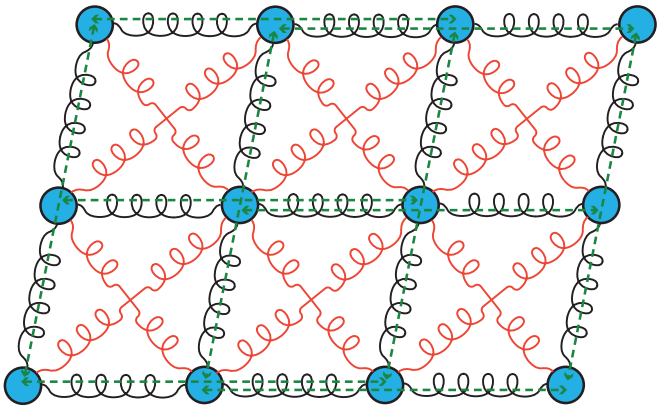

FIG. 1. (Color online) The model with nearest-neighbor (black springs), next-nearest-neighbor (red springs), and third-nearest-neighbor (dashed green lines) interactions.

Our simulations follow the tradition of large-scale simulations with open- (free-) boundary conditions and interatomic potentials.[18,20–23] Periodic boundary conditions are not used because domain boundaries have been observed to nucleate as needle domains from the crystal surface,[10,21] which obviously cannot be seen in simulations using periodic boundary conditions. In our simulations, we observed this nucleation process and also the disappearance of needle domains and kinks in domain walls into the crystal surface so that the lack of periodic boundary conditions is justified. The computer code LAMMPS was used with an NVT ensemble.

The calculated cell has one million particles and contains two buffer layers at the top and bottom of the two-dimensional sheet. These buffer layers were sheared by the external boundary conditions (fixed external strain, hard boundary conditions). Limited computer power restricts us to simulations in two dimensions. From the mean-field approximation, we believe that this choice is reasonable because it was shown previously that the addition of further layers did not change the microstructures significantly.[18] We have not tested the results for bulk materials with thicknesses of the same order of magnitude as the lateral dimensions. A study of three-dimensional materials would be highly desirable but also extremely costly in computer time.

The initial condition contained a simple twin configuration for the hard material [$K1 = 20$, Fig. 2(a)] and a sandwich configuration for both, a hard material [$K1 = 20$, Fig. 2(b)] as well as a soft material [$K1 = 10$, Fig. 2(c)]. The parameters in the potential were chosen to give an initial shear angle of 2.86°. The system was then relaxed using a conjugate gradient refinement procedure to find the optimal position for each lattice point and a modified shear angle. Molecular dynamics was then performed to anneal each configuration at a given temperature for 10^6 time steps. In all cases, the only relaxations that occurred during this procedure were surface relaxations; no further microstructures developed. After this relaxation, external strain was applied via a global shear of the two boundary layers. The shear was performed slowly over 2×10^8 time steps, while the temperature of the sample was held constant by the Nosé-Hoover thermostat.[24] For comparison, the time scale of phonon excitation (one vibration) was about 1000 time steps.

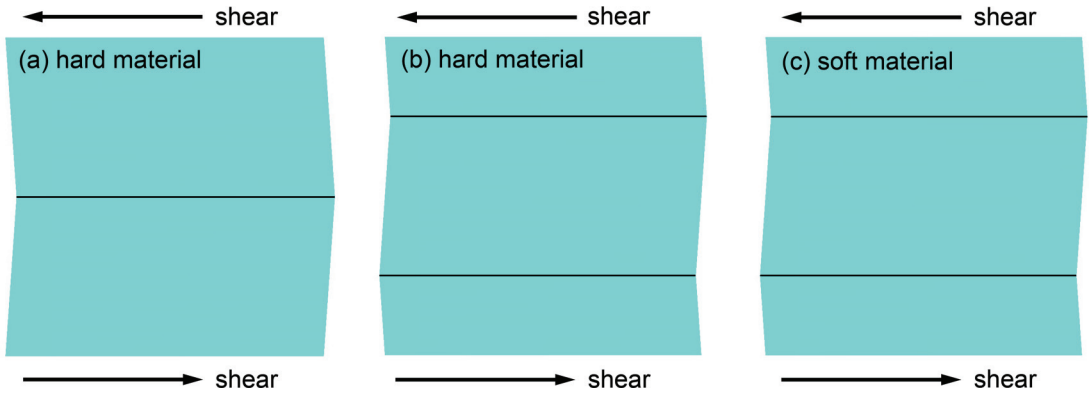

FIG. 2. (Color online) The initial configurations used in our calculation. (a) Hard material with simple twin configuration, (b) hard material with sandwich twin configuration, and (c) soft material with sandwich twin configuration.

III. RESULTS

For all the three configurations shown in Fig. 2, the response of the potential energy for the different systems to the applied strain is similar. Specifically, considering the hard material with the initial sandwich configuration [Fig. 2(b)] as an example, increasing applied strain is initially compensated by an elastic deformation until a threshold is reached (point A in Fig. 3), after which the potential energy drops dramatically. This is followed by a plateau in which detwinning occurs. With further loading, the potential energy increases again, which indicates that most of the detwinning process has been completed (after point C in Fig. 3), and the deformation is mainly from the elastic deformation of the obtained domain.

In the elastic regime, for strains below point A in Fig. 3, we find a remarkable structural instability. In sandwich configurations [Fig. 2(b) and Fig. 2(c)], we observe the formation of dynamic tweed, a flickering (i.e., dynamic change of the pattern over short time scales) cross-hatched pattern, as shown in Fig. 4(a). In contrast to static- or disorder-induced tweed due to compositional variations in which the tweed direction is the same as the elastically soft direction for the transformation, the orientation of the tweed pattern here is not in the direction of the twin boundaries. In the simple twin configuration [Fig. 2(a)], we find no dynamic tweed but simply the advance of the stable domain wall via kink propagation at the interface [Fig. 4(b)]. Further calculations show that the evolution of microstructure in the elastic regime is almost the same at different temperatures. The difference in the evolution of microstructure between the simple twin and sandwich configuration arises from the distribution of stress for twinning in the configuration under a given external shear. Once the external strain was applied via a global shear of the two boundary layers, as shown in Fig. 2, the distribution of stress for twinning in the simple twin configuration is not homogeneous, and the maximum stress lies at the corner of the simple twin model. Thus, needle domains nucleate at the corner at very early stage and propagate to the free surface at the other end. In contrast, the sandwich configuration deforms more uniformly under global shear (Fig. 2); thus, dynamic tweed is nucleated for the detwinning process, which is similar to the dynamic tweed prior to temperature-induced martensitic transformation.[17,22]

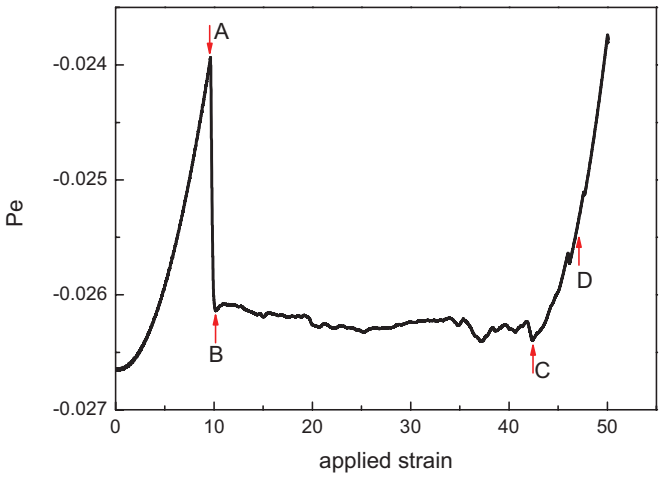

FIG. 3. (Color online) Potential energy (Pe) versus applied strain (ε) curve for the hard material with sandwich twin configuration under applied shear strain at high temperature 1.25 T_{VF} (here and elsewhere, T_{VF} refers to the Vogel-Fulcher temperature for the hard material with a simple twin configuration).

In the plastic regime after yield, for strains between point A and point C in Fig. 3 and for all the three configurations in Fig. 2 at high temperature (1.25 T_{VF}, here and elsewhere, T_{VF} refers to the Vogel-Fulcher temperature for the hard material with simple twin configuration, which is determined by the statistics in the plastic region), we find that the unstable domain in the elastic regime collapses into a multitude of twinned nanodomains over a very small strain regime (from point A to B). The domain patterns formed at point B (Fig. 3) are shown in Figs. 5(a), 5(c), and 5(e). These twin patterns do not change unless we shear further, and they are stable due to a balance between external and internal forces. The patterns will decay due to the nucleation of kinks formed in the twin boundary. Similar to that in Ref. 8, the kinks will propagate to the surface through a stick-and-slip mechanism, where the intersections of the horizontal and vertical twins leads to pinning that can be overcome by increasing a control parameter such as the macroscopic shear. As a result, the twin boundary will move down the sample and lead to the occurrence of detwinning. It is this process that leads to the elimination of twin patterns formed in the sample. However, the formed twin patterns

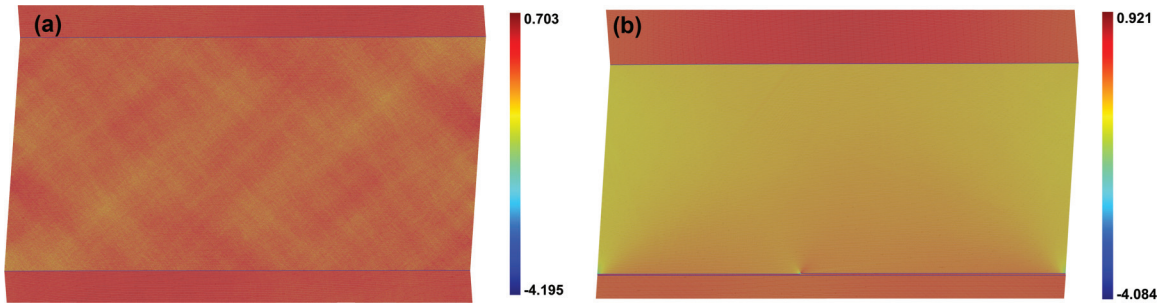

FIG. 4. (Color online) The microstructural evolution in the elastic regime (before point A in Fig. 3). (a) The dynamic tweed formed in the hard and soft materials with sandwich twin configuration [see Figs. 2(b) and 2(c)]. (b) Nucleation and propagation of needle twins in the hard material with simple twin configuration. The behavior in the elastic regime is independent of the temperature of the system. The color scheme represents the local shear angle from the underlying bulk structure ($|\Theta_{\text{vertical}}| - 4^\circ + \Theta_{\text{horizontal}}$); for details, see Ref. 8.

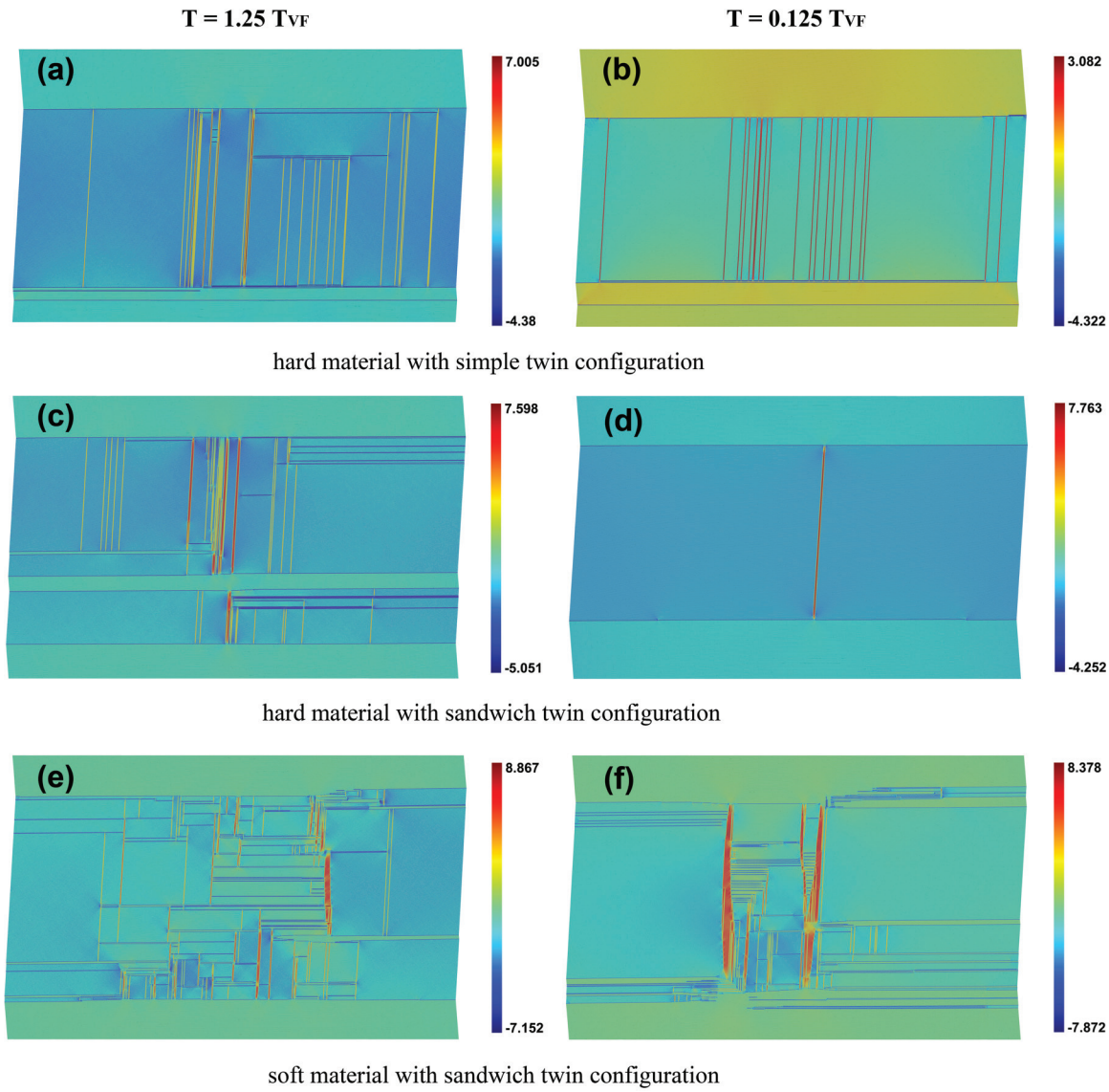

FIG. 5. (Color online) Twin patterns at low yield point (e.g., point B in Fig. 3). The twin density decreases with temperature for the hard material but not significantly for the soft material. Shown are domains formed at high temperature (a), (c), and (e) and low temperature (b), (d), and (f). Here, (a) and (b) are for hard materials with simple twin configuration; (c) and (d) show those for a hard material with the sandwich twin configuration, and (e) and (f) are for a soft material with the sandwich configuration. The color scheme represents the local shear angle from the underlying bulk structure ($|\Theta_{\text{vertical}}| - 4^\circ + \Theta_{\text{horizontal}}$); for details, see Ref. 8.

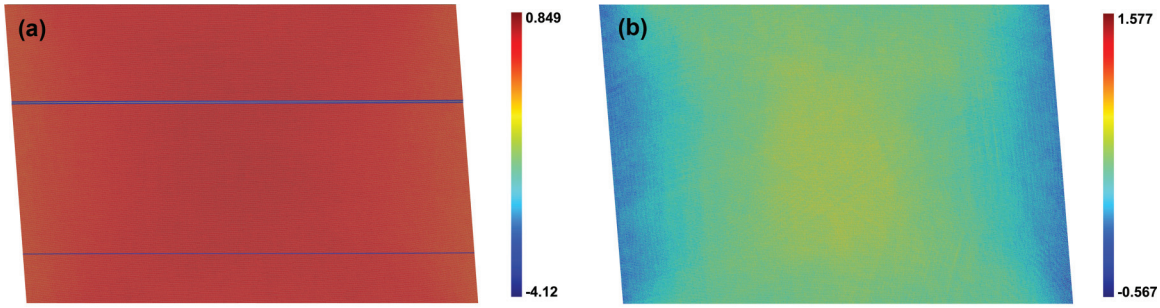

FIG. 6. (Color online) Microstructure at and after point C in Fig. 3. At point C, most of the region has been switched to the new orientation (a); further loading will lead to a perfect single domain at point D. The above behavior is independent of the configurations we used (in Fig. 2). The color scheme represents the local shear angle from the underlying bulk structure ($|\Theta_{\text{vertical}}| - 4^\circ + \Theta_{\text{horizontal}}$); for details, see Ref. 8.

are very sensitive to the change in temperature. As shown in Figs. 5(b), 5(d), and 5(f), when the system is cooled to a lower temperature (0.125 T_{VF}), the twin pattern in hard materials for both simple twin and sandwich twin configurations changes, and the density of twin boundaries decreases dramatically; whereas the twin density in soft materials with sandwich twin configuration does not change much.

When the applied strain reaches point C in Fig. 3, we find the detwinning process is almost complete, except for a small region to the left [Fig. 6(a)]. Further loading leads to a detwinning process in the remaining region, and finally the system changes to a perfect single domain crystal [as shown by point D in Fig. 3 and Fig. 6(b)].

We now analyze the energy distribution of the jerks in the plastic regime between point B and C in Fig. 3. The obtained potential energy (Pe) versus applied strain (ε) curves for the three configurations in Fig. 2 are further analyzed in terms of jerk energy. We resort to measurements of the squared first derivative of Pe as a function of the applied strain ε and then calculate the probability $P(E)$ to find jerks at a given energy E. The details on the statistics of jerks are described in Ref. 8. We find three major regimes of jerk distribution (Figs. 7 and 8) with change of temperature. The first regime is at high temperatures, where thermal excitations lead to the Vogel-Fulcher behavior of the energy distribution of jerks. The left panels of Figs. 7(a), 7(c), and 7(e) show a simple exponential distribution of $P(E)$ for hard and soft materials with simple twin and sandwich twin configurations. The thermal behavior does not differentiate between the configurations. At lower temperatures (0.125 T_{VF}), the distribution functions for the above three configurations, as shown in the right panels of Figs. 7(b), 7(d), and 7(f), change to a generalized Poisson distribution $P(E) \sim E^{-(\gamma-1)}$ exp-$(E/E_0)^n$, where the stretching exponent n is surprisingly robust in our simulations. The stretching exponent n is 0.4, and $\gamma - 1$ is close to 0. At very low temperatures, we can even see that the energy distributions of the jerks $P(E)$ in the plastic regime show power-law behavior $P(E) \sim E^{-(\gamma-1)}$, where the exponent $\gamma - 1 = 1.81$ for the hard material with simple twin configuration at 8.75×10^{-2} T_{VF} [Fig. 8(a)]; $\gamma - 1 = 2.07$ for the hard material with sandwich twin configuration at 1.25×10^{-2} T_{VF} [Fig. 8(b)], and $\gamma - 1 = 1.77$ for the soft material with sandwich twin configuration at 1.25×10^{-2} T_{VF} [Fig. 8(c)].

The waiting time between jerks was characterized by the strain intervals that also indicate the time intervals, as the applied shear speed is constant. The threshold for the jerks was set by the maximum strain interval between adjacent jerks corresponding to the largest $P(E)$ in Figs. 7(a), 7(c), and 7(e). We find that the waiting time distribution depends on the initial conditions. For example, Fig. 9 shows the waiting time of jerks at high temperature (1.25 T_{VF}). We find the waiting time of jerks in sandwich configurations (with hard and soft materials) follows simple exponential distributions [$P(\tau) \sim$ exp-(τ/τ_0)], which indicates no correlations between the jerks at high temperatures [Figs. 9(b) and 9(c)]. In the case of the hard material with simple twin configuration, the distribution is described well by a stretched exponential [$P(\tau) \sim$ exp-$(\tau/\tau_0)^n$] with a stretching exponent $n = 0.43$ [Fig. 9(a)]. In general, we can conclude that the observed waiting times statistics obey a generalized Poisson distribution[6] $P(t) \sim t^{-(\gamma-1)}$ exp-$(t/\tau)^n$ with some systems following simple exponential distributions[7] with $\gamma - 1 \approx 0$ and $n = 1$ and others following the stretched exponential with $\gamma - 1 \approx 0$ and $n = 0.4$.

We also analyzed the probability function for the jerks in the elastic regime. It is the energy fluctuations rather than the structural features that lead to the energy jerks. We found that the probability functions are sensitive to the temperature and the configurations we used. At high temperatures (1.25 T_{VF}), the energy distribution of jerks for the hard material with a simple twin model follows power law [Fig. 10(a)], whereas the energy distribution of jerks for the sandwich configurations (with hard and soft materials) follows Poisson distributions $P(E) \sim E^{-(\gamma-1)}$exp-$(E/E_0)^n$ [Figs. 10(c) and 10(e)]. At low temperatures (0.125 T_{VF}), the energy distribution of jerks for the hard material with simple twin model is erratic [Fig. 10(b)], whereas it follows a power-law behavior ($P(E) \sim E^{-(\gamma-1)}$) [Figs. 10(d) and 10(f)] for the sandwich configurations with exponents $\gamma - 1 = 1.77$ for the hard material [Fig. 10(d)] and 1.53 for the soft material [Fig. 10(f)], respectively.

Our findings show that the statistics of jerk energy in the elastic regime can be quite different from the plastic regime for a given temperature. For the sandwich twin configurations at low temperature (0.125 T_{VF}), both hard and soft materials show a distribution of jerk energy following the power law in the elastic regime, whereas noise in the plastic regime follows a stretched exponential distribution. In particular, the

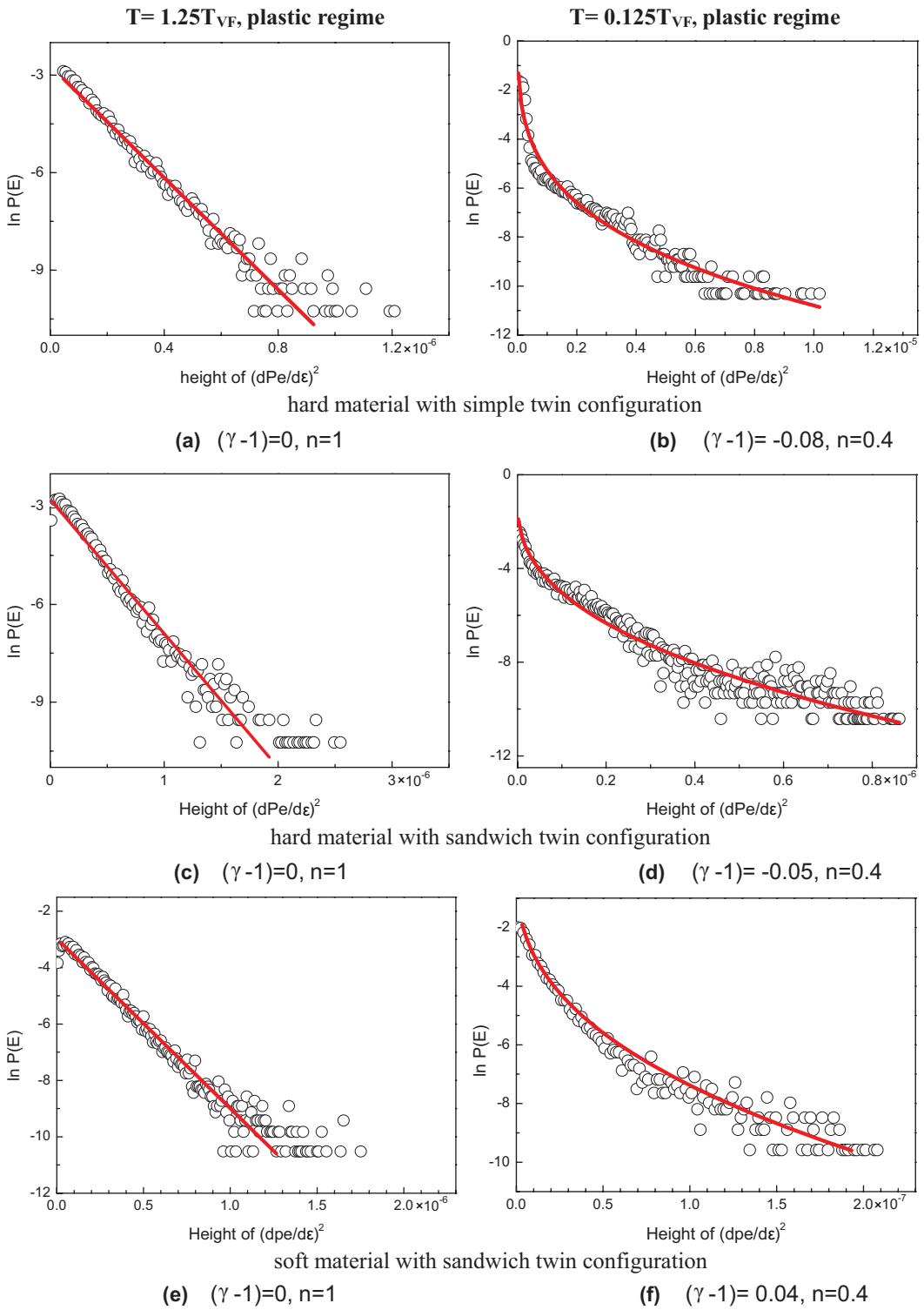

FIG. 7. (Color online) Energy distributions of jerks $P(E)$ in the plastic regime at high (1.25 T_{VF}) and low temperatures (0.125 T_{VF}) that show that the energy distributions of the jerks depend on temperature, whereas they are not sensitive to the configurations we used. The energy distributions of the jerks at high temperature (1.25 T_{VF}) for the three configurations (a), (c), and (e) follow simple exponential distributions, whereas those (b), (d), and (f) at lower temperatures (0.125 T_{VF}) show Poisson distributions $P(E) \sim E^{-(\gamma-1)}\exp\text{-}(E/E_0)^n$ with stretching exponent $n = 0.4$.

characteristic geometrical patterns change from being dynamic in the elastic regime [Fig. 4(a)], to the interpenetrating needle domains (Fig. 5) in the plastic regime that are subsequently eliminated under increasing strain.

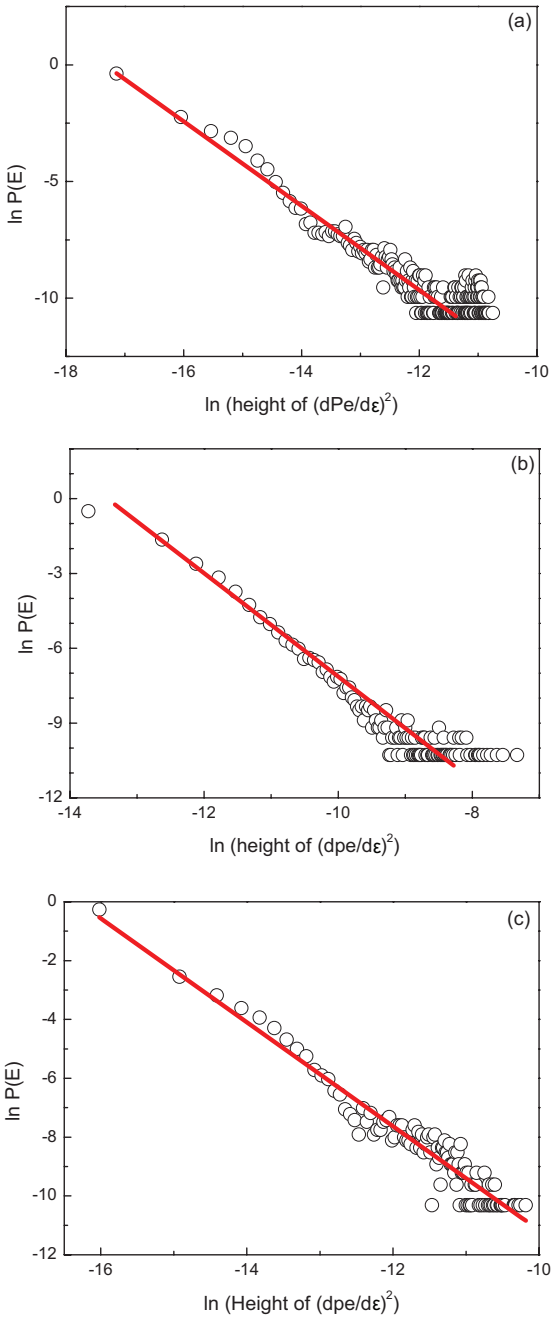

FIG. 8. (Color online) At very low temperature, the energy distributions of the jerks $P(E)$ in the plastic regime show power-law behavior $P(E) \sim E^{-(\gamma-1)}$, where (a) the exponent $\gamma - 1 = 1.81$ for the hard material with simple twin configuration for $8.75 \times 10^{-2}\ T_{VF}$; (b) $\gamma - 1 = 2.07$ for the hard material with the sandwich twin configuration for $1.25 \times 10^{-2}\ T_{VF}$ and (c) $\gamma - 1 = 1.77$ for soft material with the sandwich twin configuration for $1.25 \times 10^{-2}\ T_{VF}$.

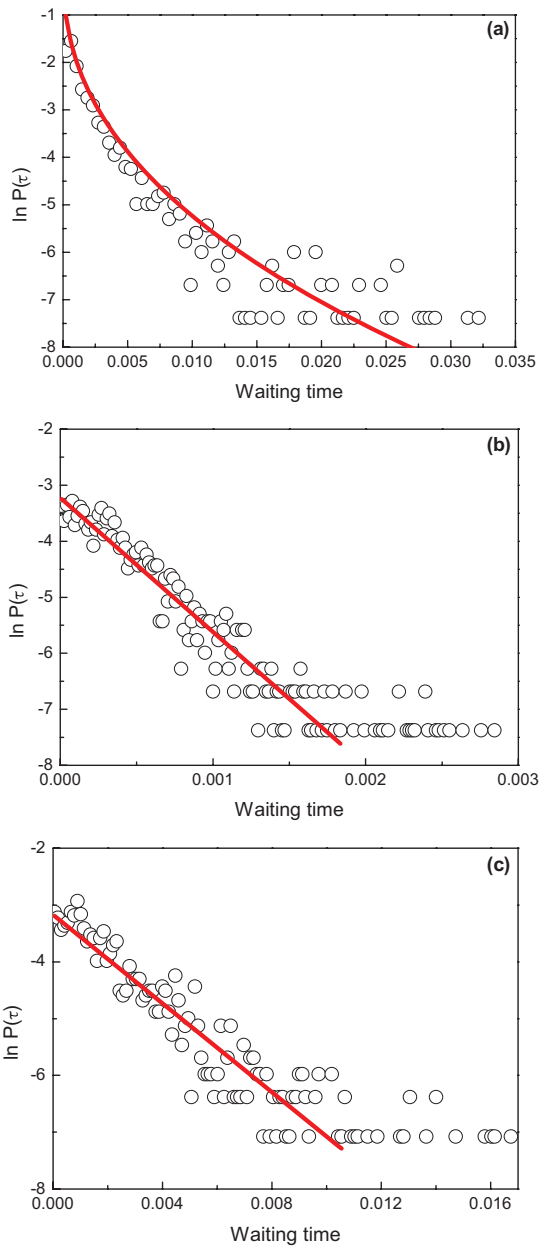

FIG. 9. (Color online) At high temperature ($1.25\ T_{VF}$), the waiting time in the plastic regime for all considered different materials follows the stretched exponential $P(\tau) \sim \exp\text{-}(\tau/\tau_0)^n$, where (a) $n = 0.43$ for a hard material with double-twin configuration, (b) $n = 1$ for the hard material with a sandwich configuration, and (c) $n = 1$ for the soft material with sandwich configuration.

IV. DISCUSSION

We first compare our results with theoretical predictions. As in most pattern formation processes, scaling emerges as an interplay between quenched disorder (quenched at the yield point), fast dynamics of the propagating twin walls, and the slow driving by the prescribed strain on the macroscopic sample. Two different regimes are theoretically expected. In models of disorder, such as the random-field Ising model, the strength of disorder determines the dynamic response, which besides singular points, is not scale invariant.[25] The pattern evolution is dominated by nucleation and destruction of the patterns by the advancing stable domain. The second scenario links criticality to the pinning-unpinning process, which is observed experimentally for advancing single-needle domains. This scenario is also referred to as the stick-and-slip mechanism of twin boundary movement, where each defect leads to pinning that can be overcome by increasing a control parameter such as the macroscopic shear. In this case, the jerks are exclusively related to the propagation of walls.

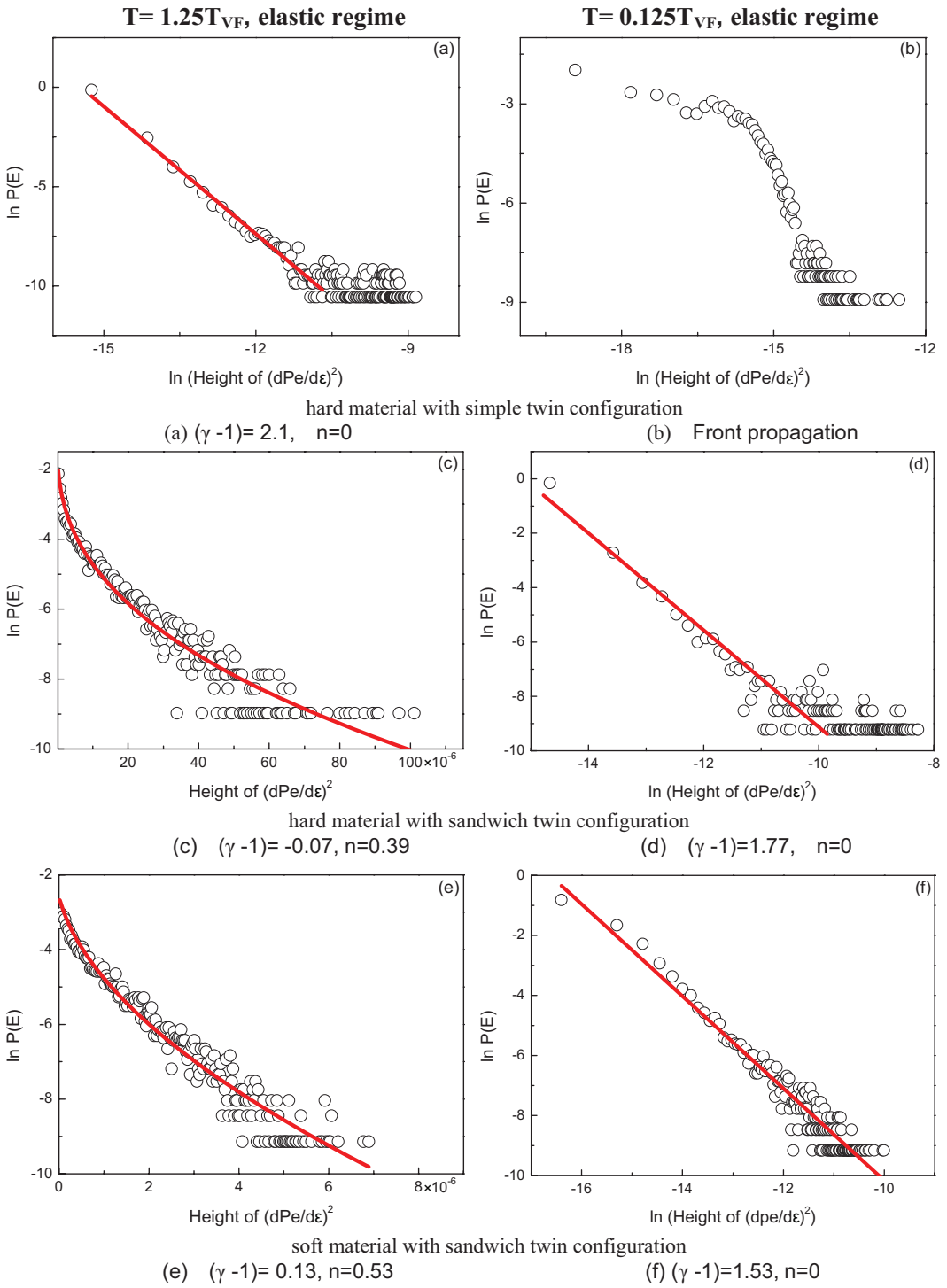

FIG. 10. (Color online) Energy distributions of jerks $P(E)$ in the elastic regime at high (1.25 T_{VF}) and low temperature (0.125 T_{VF}), which show the energy distributions of jerks in the elastic regime is very sensitive to both the temperature and the configurations we used. The left column shows results at high temperature (1.25 T_{VF}), The energy distribution of the jerks for (a) the hard material with the simple twin configuration shows power-law distribution $P(E) \sim E^{-(\gamma-1)}$ with an exponent $\gamma - 1$ of 2.1, whereas (c) hard and (e) soft materials with sandwich configuration only show Poisson distributions $P(E) \sim E^{-(\gamma-1)}\exp\text{-}(E/E_0)^n$, in which $(\gamma - 1) = -0.07, n = 0.39$ and $(\gamma - 1) = 0.13$, $n = 0.53$, respectively. The right column shows results at low temperature (0.125 T_{VF}). The energy distributions of jerks for (b) a hard material with simple twin configuration is erratic (local front propagation), whereas (d) hard and (f) soft materials with sandwich twin configuration show power-law distributions $P(E) \sim E^{-(\gamma-1)}$ with the exponent $\gamma - 1$ of 1.77 and 1.53, respectively.

A clear distinction between these scenarios was highlighted in Ref. 25, and the relevant cases were discussed there. Our simulations confirm this result: elastic systems below the yield point at low temperatures show dynamic patterns

with power-law distributions of jerks, whereas at the yield point, and in the plastic regime, a disordered twin pattern follows a Kohlrausch law. The thermal region between the low-temperature regime (power law) and the high-temperature regime (Vogel-Fulcher regime) is traditionally described by power laws with decreasing cutoff lengths[26] (our increasing temperature). The scaling function is undefined in the approach of Ref. 26 and, as it turns out by numerical fits, is often exponential. In our analysis, we follow a different route: we describe the entire probability distribution for avalanches by one functional form (the generalized Poisson distribution). The advantage of this approach is that all three regions (power law, stretched exponential, and Vogel-Fulcher) can be cast in the same functional form. We showed that the tendency is similar to the previous analysis using cutoff lengths: the power law dominates the low-temperature regime and the exponential part increases with increasing temperature. The intermediate regime is surprisingly well described by a stretched exponential (Kohlrausch law). We note that the energy fluctuations are larger in the elastic regime, which shows either the formation of dynamic tweed or the nucleation of needle domains from the surface (Fig. 3). The fluctuations become smaller in the plastic regime. This behavior was anticipated in Ref. 25.

We note that the present statistical analysis is limited to specific regions of the strain-stress curves.[2–4] Spatial correlations cannot be analyzed in the collapse region (between points A and B in Fig. 3) because this interval is too narrow and only few events occur so that no statistical analysis is meaningful. In the elastic regime (from the start to point A in Fig. 3), the flickering tweed is highly dynamic and correlation functions need to include frequency constraints. Only the static average is known for such microstructures, the evaluation of the dynamical correlations in this regime is extremely difficult and has not been attempted. The obvious regime for a detailed analysis is the plastic regime (between points B and C in Fig. 3). Here, all correlations are known and jerks are related to the pinning and depinning events. The (de)pinning relates to not only the needle domains in the main but also to kinks in twin boundaries. The statistical analysis hence has these events as physical background.

We now comment on the existence of the stretched exponential regime (Kohlrausch law), which we introduced in this paper for the first time for the description of avalanche statistics at intermediate temperatures. The Kohlrausch law is ubiquitously encountered in disordered systems.[27] Examples include glassy and polymeric materials,[28] electric polarization[29] and electric birefringence,[30] supercooled liquids,[4] molecular and electronic glasses,[31] and Lennard-Jones systems.[32] They have been discussed in detail in Ref. 31. The stretching exponent of about 0.5 occurs frequently and Huse and Fisher[33] derived the correlation functions for a defect-free Ising model with no conservation laws constraining its dynamics. They found a "stretched exponential" $C(t) \sim \exp\,[-(t/\tau)^{0.5}]$ in a two-dimensional system related to droplet formation. A more general analysis by Nemeth[34] showed a competition between power law and stretched exponential distributions for Ising models, the equivalent stretching exponent remains 0.5. In addition, Stauffer[35] found stretched exponentials in two dimensions but not in three dimensions. Alternatively, stretched exponentials with n near 0.5 can be derived from even more general arguments[36] when exponential relaxations are averaged over a susceptibility function related to independent excitations in a Maxwell distribution of weakly interacting states. Similar stretched exponentials were also observed in random-field Ising models by Young,[37] who argued that the typical on-site time-dependent correlation function decays with a stretched exponential behavior with a stretching exponent $1/2.2 = 0.45$. Dynamic stretching exponents in the Sherrington-Kirkpatrick Ising spin glass were found to be 0.33.[38]

In a comprehensive review, Phillips[4] showed that in many scenarios the stretching exponent is $\beta = d/(\mathrm{d}+2)$, where d is the dimension of the system (in our case $d = 2$, $\beta = 0.5$). The two major contexts are within the scope of the hydrodynamic model[39] and the trapping model.[40–42] Whereas the hydrodynamic model cannot derive β, it can nevertheless link β to the dynamic excitations in glasses and can provide a general framework for the understanding of the existence of stretching exponents in "glass-like" materials. The trapping model is more predictive. Starting from a diffusion process in the presence of randomly distributed "traps" and a cutoff length scale for the trapping distance, one finds the probability that a particle at a distance R from the traps has survived until time t. The survival probability follows the Kohlrausch law in time with a stretching exponent $\beta = d/(d+2)$.[42] Much discussion has followed to restrict this conclusion to specific (small) trap densities. In our simulations, the diffusing species are kinks in twin walls and sideways movements of walls. The trap density is then given by the number of junctions between walls, which is a small percentage of the particle number. While the trap model was not designed specifically for the annealing of microstructures, it seems that its predictions are relevant and shed some light on the trapping statistics of twin walls in a complex pattern generated at the yield point. In this model, the junctions act as trapping centers and the moving defects are the twin walls. The statistical behavior of the twin wall avalanches follows then, at intermediate temperatures, the predictions of the trapping model.

In a review, Kleemann[43] showed that it is relatively easy to analyze domain-wall dynamics under electric fields and put much emphasis on the crossover between the creep regime and the depinning regime of a domain wall. Only very few experimental studies of the equivalent mechanical forcing of the wall movements have been undertaken,[44] which is partly due to the experimental difficulties in measuring the inelastic response and to observe the twinning pattern in the sample.[45] In cases in which the depinning behavior has been observed, one finds very similar depinning exponents ($\sim$0.5) as in magnetic materials but not in ferroelectrics, where the exponents are closer to one.[46] Similarly, the slow creep regime is well established in magnetic and ferroelectric materials but much less in ferroelastic and martensitic materials. Our results confirm a similar picture: the smooth ballistic movement of twin walls does, in principle, exist and gives rise to creep and depinning dynamics.[17] The overall dynamics under hard boundary conditions (fixed external strain) is dominated by rapid nucleation of intricate twin patterns near the yield point and, under subsequent shear, by avalanches during the destruction of the unstable twin

orientation. In virtually no case do we observe ballistic movement of individual walls beside short-time movements of kinks inside domain walls, however. The dynamics is mostly related to the nucleation and destruction of collective twin assemblies.

Dynamics of ferroelectric walls have also been investigated in some detail.[46] The nucleation and growth of domain patterns is then described by stretched exponentials similar to our results. The most direct comparison is possible in $PbZr_{0.2}Ti_{0.8}O_3$,[47] where the dominant contribution to the lateral piezoelectric signal is due to domain walls. These walls are ferroelastic, and our analysis could provide a means to produce samples with much higher domain boundary densities. These may be generated in the way described, namely, by shear under hard boundary conditions. The dynamics of dense walls was observed in $BaTiO_3$ where a stretched exponential behavior with β approaching 0.5 for small driving electric fields was found.[48]

An interesting comparison is also with Barkhausen jumps in CrO_2, which is a useful material for ferromagnetic applications,[49] where the dynamics is dominated by avalanches rather than ballistic wall movements. Unfortunately, the noise exponents were not determined so that we cannot compare these data with ours.

In summary, stretched exponential Kohlrausch laws have been observed in a multitude of scenarios. The same analysis works equally well for avalanches in ferroelastic materials at intermediate temperatures and provides a natural interpolation between the power law and Vogel-Fulcher law at low and high temperatures.

ACKNOWLEDGMENTS

X.D., Z.Z., and J.S. appreciate the support of the Natural Science Foundation of China (No. 51171140 and No. 51231008), the National Basic Research program of China (No. 2010CB631003 and No. 2012CB619402), and the Program of Introducing Talents of Discipline to Universities in China (No. B06025). E.K.H.S. is grateful to the Leverhulme Foundation and the Engineering and Physical Sciences Research Council for support. This work was supported in part by US Department of Energy at Los Alamos National Laboratory (No. DE-AC52-06NA25396).

*Corresponding authors: ekhard@esc.cam.ac.uk; dingxd@mail.xjtu.edu.cn

[1] P. C. Hohenberg and B. I. Halperin, Rev. Mod. Phys. **49**, 435 (1977).
[2] J. P. Sethna, K. A. Dahmen, and C. R. Myers, Nature (London) **410**, 242 (2001).
[3] N. Friedman, S. Ito, B. A. W. Brinkman, M. Shimono, R. E. Lee DeVille, K. A. Dahman, J. M. Beggs, and T. C. Butler, Phys. Rev. Lett. **108**, 208102 (2012).
[4] J. C. Phillips, Rep. Prog. Phys. **59**, 1133 (1996).
[5] E. K. H. Salje, D. E. Soto-Parra, A. Planes, E. Vives, M. Reinecker, and W. Schranz, Philos. Mag. Lett. **91**, 554 (2011); M. C. Gallardo, J. Manchado, F. J. Romero, J. del Cerro, E. K. H. Salje, A. Planes, E. Vives, R. Romero, and M. Stipcich, Phys. Rev. B **81**, 174102 (2010); E. K. H. Salje, J. Koppensteiner, M. Reinecker, W. Schranz, and A. Planes, Appl. Phys. Lett. **95**, 231908 (2009).
[6] F. J. Romero, J. Manchado, J. M. Martin-Olalla, M. C. Gallardo, and E. K. H. Salje, Appl. Phys. Lett. **99**, 011906 (2011).
[7] G. Niccolini, A. Carpinteri, G. Lacidogna, and A. Manuello, Phys. Rev. Lett. **106**, 108503 (2011).
[8] E. K. H. Salje, X. Ding, Z. Zhao, T. Lookman, and A. Saxena, Phys. Rev. B **83**, 104109 (2011).
[9] X. Ding, Z. Zhao, T. Lookman, A. Saxena, and E. K. H. Salje, Adv. Mater. **24**, 5385 (2012).
[10] E. K. H. Salje, *Phase Transitions in Ferroelastic and Co-Elastic Crystals* (Cambridge University Press, Cambridge, 1993).
[11] J. K. Deng, X. D. Ding, T. Lookman, T. Suzuki, K. Otsuka, J. Sun, A. Saxena, and X. Ren, Phys. Rev. B **81**, 220101 (2010); X. D. Ding, T. Suzuki, X. B. Ren, J. Sun, and K. Otsuka, *ibid.* **74**, 104111 (2006).
[12] M. Porta, T. Castan, P. Lloveras, T. Lookman, A. Saxena, and S. R. Shenoy, Phys. Rev. B **79**, 214117 (2009); R. Groger, T. Lookman, and A. Saxena, *ibid.* **78**, 184101 (2008).
[13] E. Salje, B. Palosz, and B. Wruck, J. Phys. C: Solid State Phys. **20**, 4077 (1987); A. Froseth, H. Van Swygenhoven, and P. M. Derlet, Acta Mater. **52**, 2259 (2004).
[14] G. Boussinot, Y. Le Bouar, and A. Finel, Acta Mater. **58**, 4170 (2010); A. Gaubert, Y. Le Bouar, and A. Finel, Philos. Mag. **90**, 375 (2010).
[15] A. E. Jacobs, Phys. Rev. B **61**, 6587 (2000).
[16] E. Salje and K. Parlinski, Supercond. Sci. Technol. **4**, 93 (1991).
[17] E. K. H. Salje, Chem. Phys. Chem. **11**, 940 (2010).
[18] K. Parlinski, E. K. H. Salje, and V. Heine, Acta Metall. Mater. **41**, 839 (1993).
[19] E. K. H. Salje, M. C. Gallardo, J. Jimenez, F. J. Romero, and J. D. Cerro, J. Phys.: Condens. Matter **10**, 5535 (1998).
[20] S. Conti and E. K. H. Salje, J. Phys.: Condens. Matter **13**, L847 (2001).
[21] J. Novak and E. K. H. Salje, Euro. Phys. J. B **4**, 279 (1998); J. Phys.: Condens. Matter **10**, L359 (1998); J. Novak, U. Bismayer, and E. K. H. Salje, *ibid.* **14**, 657 (2002).
[22] A. M. Bratkovsky, S. C. Marais, V. Heine, and E. K. H. Salje, J. Phys.: Condens. Matter **6**, 3679 (1994); A. M. Bratkovsky, E. K. H. Salje, S. C. Marais, and V. Heine, Phase Transitions **48**, 1 (1994).
[23] K. Parlinski, V. Heine, and E. K. H. Salje, J. Phys.: Condens. Matter **5**, 497 (1993).
[24] S. Nose, J. Chem. Phys. **81**, 511 (1984); W. G. Hoover, Phys. Rev. A **31**, 1695 (1985).
[25] F.-J. Pérez-Reche, L. Truskinovsky, and G. Zanzotto, Phys. Rev. Lett. **101**, 230601 (2008).
[26] Y. Ben-Zion, K. A. Dahmen, and J. T. Uhl, Pure Appl. Geophys. **168**, 2221 (2011).
[27] W. T. Coffey and Yu. P. Kalmykov, *Fractals, Diffusion and Relaxation in Disordered Systems* (Wiley-Interscience, New York, 2006); G. Williams and D. C. Watts, Trans. Faraday Soc. **66**, 80 (1970).
[28] G. Kriza and G. Mihály, Phys. Rev. Lett. **56**, 2529 (1986).
[29] V. Degiorgio, T. Bellini, R. Piazza, F. Mantegazza, and R. E. Goldstein, Phys. Rev. Lett. **64**, 1043 (1990).
[30] P. K. Dixon, L. Wu, S. R. Nagel, B. D. Williams, and J. P. Carini, Phys. Rev. Lett. **65**, 1108 (1990).

[31]E. Rabani, J. D. Gezelter, and B. J. Berne, Phys. Rev. Lett. **82**, 3649 (1999).
[32]I. Eliazar and J. Klafter, Phys. Rep. **511**, 143 (2012).
[33]D. A. Huse and D. S. Fisher, Phys. Rev. B **35**, 6841 (1987).
[34]R. Nemeth, Physica A **169**, 444 (1990).
[35]D. Stauffer, Physica A **186**, 197 (1992).
[36]E. K. H. Salje and B. Wruck, Phys. Chem. Miner. **16**, 140 (1988).
[37]A. P. Young, Phys. Rev. B **56**, 11691 (1997).
[38]A. Billoire and I. A. Campbell, Phys. Rev. B **84**, 054442 (2011).
[39]W. Gotze and L. Sjogren, Rep. Prog. Phys. **55**, 241 (1992).
[40]I. M. Lifshitz, Sov. Phys. Usp. **7**, 549 (1965).
[41]R. Friedberg and J. M. Luttinger, Phys. Rev. B **12**, 4460 (1975).
[42]M. D. Donsker and S. R. S. Varadhan, Commun. Pure Appl. Math. **28**, 525 (1975).
[43]W. Kleemann, Annu. Rev. Mater. Res. **37**, 415 (2007).
[44]R. J. Harrison and E. K. H. Salje, Appl. Phys. Lett. **99**, 151915 (2011); **97**, 021907 (2010); R. J. Harrison, S. A. T. Redfern, and E. K. H. Salje, Phys. Rev. B **69**, 144101 (2004).
[45]R. J. Harrison, S. A. T. Redfern, A. Buckley, and E. K. H. Salje, J. Appl. Phys. **95**, 1706 (2004).
[46]C. S. Ganpule, V. Nagarajan, S. B. Ogale, A. L. Roytburd, E. D. Williams, and R. Ramesh, Appl. Phys. Lett. **77**, 3275 (2000).
[47]J. Guyonnet, H. Bea, and P. Paruch, J. Appl. Phys. **108**, 042002 (2010); R. G. P. McQuaid, M. McMillen, L. W. Chang, A. Gruverman, and J. M. Gregg, J. Phys.: Condens. Matter **24**, 024204 (2012); Y. Ivry, D. Chu, J. F. Scott, E. K. H. Salje, and C. Durkan, Nano Lett. **11**, 4619 (2011); Y. Ivry, N. Wang, D. P. Chu, and C. Durkan, Phys. Rev. B **81**, 174118 (2010).
[48]Z. Liu, A. L. Meier, and B. W. Wessels, J. Appl. Phys. **104**, 064115 (2008).
[49]P. Das, F. Porrati, S. Wirth, A. Bajpai, M. Huth, Y. Ohno, H. Ohno, and J. Müller, Appl. Phys. Lett. **97**, 042507 (2010).